Journal of Instrumentation

PAPER • **OPEN ACCESS**

Beam test studies with silicon sensor module prototypes for the CMS Phase-2 Outer Tracker

To cite this article: F. Wittig *et al* 2023 *JINST* **18** C01005

Published by IOP Publishing for Sissa Medialab

Received: *September 29, 2022*
Accepted: *November 29, 2022*
Published: *January 10, 2023*

23rd International Workshop on Radiation Imaging Detectors
26–30 June 2022
Riva del Garda, Italy

Beam test studies with silicon sensor module prototypes for the CMS Phase-2 Outer Tracker

F. Wittig,[a,*] R. Koppenhöfer,[a] S. Maier[a] and A. Nürnberg[b] on behalf of the Tracker Group of the CMS collaboration

[a] *Karlsruhe Institute of Technology, Hermann-von-Helmholtz-Platz 1, Eggenstein-Leopoldshafen, Germany*
[b] *Deutsches Elektronen-Synchrotron, Notkestraße 85, Hamburg, Germany*

E-mail: florian.wittig@kit.edu

Abstract: The Large Hadron Collider (LHC) at CERN will be upgraded to the High-Luminosity LHC (HL-LHC) by 2029. In order to fully exploit the physics potential of the high luminosity era the experiments must undergo major upgrades. In the context of the upgrade of the Compact Muon Solenoid (CMS) experiment the silicon tracker will be fully replaced. The outer part of the new tracker (Outer Tracker) will be equipped with about 13,000 double-layer silicon sensor modules with two different flavors: PS modules consisting of a macro-pixel and a strip sensor and 2S modules using two strip sensors. These modules can discriminate between trajectories of charged particles with low and high transverse momentum. The different curvature of the trajectories in the CMS magnetic field leads to different hit signatures in the two sensor layers. By reading out both sensors, matching hits in the seed and correlation layer "stubs" are identified. This stub information is generated at the LHC bunch crossing frequency of 40 MHz and serves as input for the first stage of the CMS trigger. In order to quantify the hit and stub detection efficiency, beam tests have been performed. This article comprises selected studies from measurements gathered during two beam tests at the DESY test beam facility with 2S prototype modules assembled in 2021, featuring the Low Power Gigabit Transceiver (lpGBT). In order to compare the module performance at the beginning and end of the CMS runtime, a module with irradiated components has been built and intensively tested.

Keywords: Particle tracking detectors; Radiation damage to detector materials (solid state); Radiation-hard detectors; Si microstrip and pad detectors

*Corresponding author.

https://doi.org/10.1088/1748-0221/18/01/C01005

Contents

2023 JINST 18 C01005

1 Introduction

The instantaneous luminosity of the Large Hadron Collider (LHC) at CERN will be increased up to 7.5×10^{34} cm^{-2} s^{-1} by the upgrade to the HL-LHC, resulting in about 200 proton-proton interactions per bunch crossing (pileup) on average. Before the start of the HL-LHC operation, the experiments have to be fundamentally revised to cope with the intensified particle flux. For the Compact Muon Solenoid (CMS) [1] experiment this upgrade is referred to as the Phase-2 Upgrade [2]. Replacing the complete CMS silicon-based tracker is a crucial part of the upgrade. The new tracker is required to have better radiation tolerance, higher granularity, lower material budget, and has to provide tracking information to the first CMS trigger stage. Highly granular pixel modules will be installed in the inner part of the tracker, whereas the Outer Tracker will be equipped with modules consisting of two closely spaced silicon sensors. Depending on the module position, two different types of modules will be used. 2S modules comprising two identical silicon strip sensors will be installed in the outer region and PS modules consisting of a macro-pixel and a strip sensor are intended for the inner region of the Outer Tracker. This article focuses on the 2S module.

Figure 1(a) depicts a schematic view of the 2S module design with all its main components. The silicon sensors have a size of about $10 \times 10\,\text{cm}^2$ and are segmented in two rows of 1016 strips each, with 90 μm pitch. Precise sensor spacing is achieved by gluing the sensors back to back onto two isolated bridges made of carbon fiber reinforced aluminium (Al-CF). Different bridge thicknesses are available to achieve sensor spacings of 1.8 mm or 4 mm. Two Front-End Hybrids (FEHs) are placed at opposite sides of the sensors. Each front-end hybrid is equipped with eight CMS Binary Chips (CBCs) [3] that are wire-bonded to the strips of the lower and upper sensor, reading out and processing the sensor signals. Binary data, 0 if the signal is below a programmable threshold and 1 above, from the CBC chips is compressed and serialized by the Concentrator Integrated Circuit (CIC) placed on each FEH. The Service Hybrid (SEH) accommodates a Low Power Gigabit Transceiver (lpGBT) [4], which receives and serializes the CIC data before sending it to the Versatile Transceiver Plus (VTRX+) [5] for opto-electrical conversion. An optical fiber

connects the VTRX+ with the off-module data acquisition system. Furthermore, the SEH houses DC-DC converter stages featuring the bPOL12V [6] and bPOL2V5 [7] supplying all the voltage levels required by the front-end electronics.

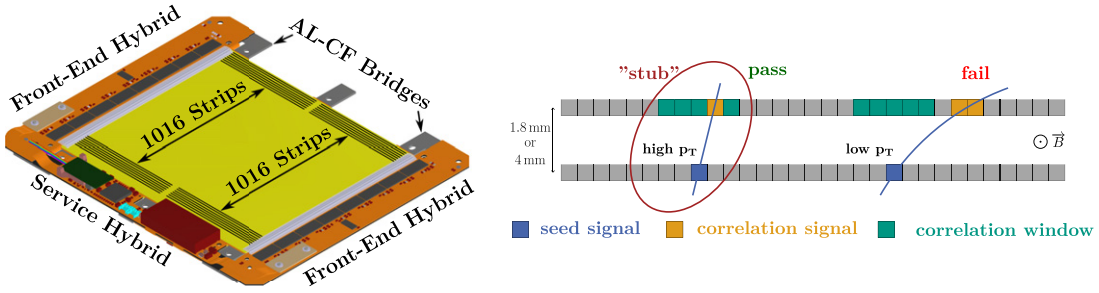

(a) (b)

Figure 1. (a) Sketch of the 2S module design showing all main components of the module. Modified from [9]. (b) Illustration of the module p_T discrimination concept.

The special design of the Outer Tracker modules featuring two closely spaced sensors allows to distinguish between particles with low and high transverse momentum (p_T). Figure 1(b) illustrates the working principle. Since the entire tracker is operated within a homogeneous magnetic field of 3.8 T, the trajectories of traversing charged particles are bent. Therefore, particles create slightly displaced hits in the two sensor layers, where the displacement depends on the particle's transverse momentum. By reading out superimposed strips with the same set of readout chips, the displacement of the hit position between the seed and correlation layer can be determined. Only if the displacement is within a programmable correlation window, whose size defines the p_T threshold, the hits are matched, forming a stub. Applying a p_T threshold of 2 GeV on the trigger input data significantly reduces the number of tracks per event [8], requiring less bandwidth for data transmission without losing interesting particles. Thus, it is possible to provide the module stub information to the track finder of the first CMS trigger stage at the LHC bunch crossing frequency of 40 MHz. Supplying tracking information to the first CMS trigger stage is a key feature of the new Phase-2 Outer Tracker and is required to efficiently select interesting events at moderate trigger rates.

For the beam test measurements presented in section 3, two 2S modules of the latest[1] prototype version have been used. One module has been built from non-irradiated components while a second one was assembled with irradiated sensors and front-end hybrids. This allows to quantify the module performance regarding the effects of radiation damage. The irradiation of the individual module components has been performed with 23 MeV protons at the Karlsruhe compact cyclotron (KAZ) [10].

[1] Within this article the term "latest" refers to 2S module prototypes assembled in 2021, featuring the Low Power Gigabit Transceiver (lpGBT).

2023 JINST 18 C01005

During the entire HL-LHC phase it is not foreseen to replace any components of the Outer Tracker. Modules have to cope with different fluences depending on the CMS detector operation time and the individual module location. The corresponding fluences can be derived from FLUKA simulations. Assuming the "nominal" scenario with about 10 years of operation and a total integrated luminosity of 3000 fb^{-1}, the maximum 2S fluence is expected to be $3.7 \times 10^{14}\,n_{eq}/cm^2$. In the "ultimate" scenario, the integrated luminosity increases to 4000 fb^{-1} resulting in an even higher maximum fluence of $4.9 \times 10^{14}\,n_{eq}/cm^2$. To probe both scenarios within one module two sensors irradiated to different fluences were used during the module assembly. Table 1 summarizes the component fluences and compares them to the expected maximum 2S fluences of the two scenarios. Only a small fraction of modules will be exposed to the maximum fluences and, thus, the irradiated module represents the worst-case scenario in terms of sensor irradiation. Annealing of radiation damage is another aspect that impacts the sensor performance regarding the charge signal. Thus, both sensors have been annealed for 140 d at room temperature, based on the expectation of two weeks of maintenance per year within the 10 years of operation, during which room temperature annealing periods are envisaged since the leakage current of the irradiated sensors will be beneficially affected. During detector operation the sensors are kept at about −20 °C. The fluence of the front-end hybrids was limited by the maximum allowed ionizing dose of the chips, which is 150 kGy.

Table 1. Fluences of the irradiated 2S module components in relation to the maximum expected fluence for 2S modules for different CMS operation scenarios. The fluences are based on FLUKA v3.7.20.1 simulation results and correspond to the nominal and ultimate scenario with maximum 2S module fluences of $3.7 \times 10^{14}\,n_{eq}/cm^2$ and $4.9 \times 10^{14}\,n_{eq}/cm^2$, respectively.

Component	Fluence	Dose	Nominal fraction	Ultimate fraction	Annealing
Top sensor	$5.2 \times 10^{14}\,n_{eq}/cm^2$	780 kGy	140%	**106%**	140 d
Bottom sensor	$3.7 \times 10^{14}\,n_{eq}/cm^2$	555 kGy	**100%**	76%	140 d
Front-end hybrids	$1 \times 10^{14}\,n_{eq}/cm^2$	150 kGy	27%	20%	—

Beam test measurements with the above introduced 2S module prototypes have been performed at the DESY test beam facility [11] in Hamburg, Germany, in June and November 2021. The facility offers three beam lines providing an electron or positron beam with adjustable particle energy of up to 6.3 GeV. Furthermore, a EUDET-like beam telescope [12] is available to reconstruct particle tracks. Figure 2(a) depicts a schematic view of the measurement setup. The telescope is divided into an upstream and a downstream arm, which can be moved along the beam axis independently of each other. Each arm consists of three planes equipped with highly granular MIMOSA pixel sensors. The device under test (DUT) is placed in between the two arms. Since the integration time of the telescope is much longer compared to the 25 ns sampling time of the 2S module, an additional timing reference plane with a sampling time identical to the 2S module is used. The trigger signal for reading out the telescope, the DUT and the reference plane is generated by coincidence of signals coming from scintillators located at the front and rear ends of the telescope.

2023 JINST 18 C01005

For data acquisition, the EUDAQ [13] framework is used, which communicates with all devices, combines the data streams and converts them into an event-based format.

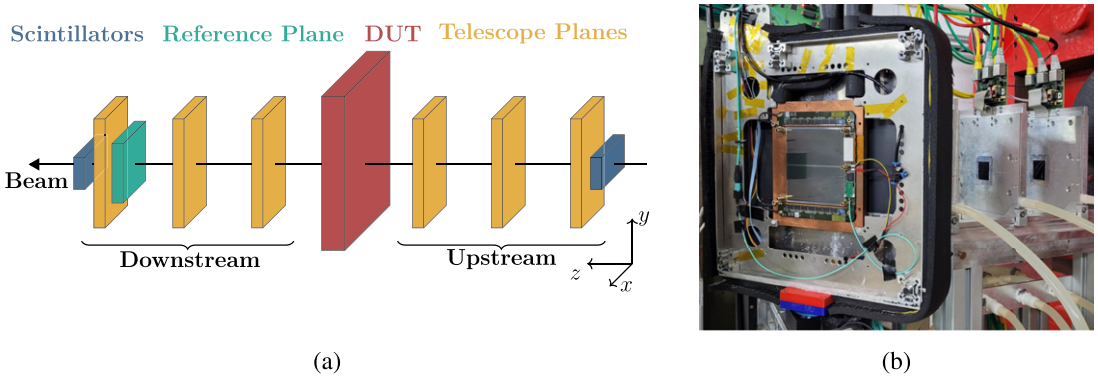

(a) (b)

Figure 2. (a) Schematic view of the beam test setup. (b) Picture of the irradiated 2S module mounted on a copper cooling bridge inside the DUT box.

The 2S module is installed inside a light-tight box that is mounted on a movement and rotation stage allowing precise positioning of the module with respect to the beam. Operating the irradiated module requires additional cooling to keep the sensor leakage currents at a moderate level, preventing thermal runaway. Thus, a copper cooling bridge connected to a chiller is installed inside the DUT box onto which the module is screwed, as shown in figure 2(b).

2 Data analysis — definitions and selection criteria

For track reconstruction the EUTelescope framework [14] has been used, offering track fitting and alignment methods based on the General Broken Line algorithm [15], which takes into account the particle energy and multiple scattering. Hit clusters are formed for each plane, whereas clusters with contributions of noisy pixels are rejected. The tracks are reconstructed based on the cluster positions at the individual telescope planes. Valid tracks are required to have a cluster in each of the six planes. Only tracks that are in coincidence with a reference plane cluster are used for the efficiency analysis.

In general, the efficiency ϵ is determined from the ratio of reference tracks matched with DUT clusters and the total number of reconstructed reference tracks

$$\epsilon = \frac{n_{\text{matched DUT tracks}}}{n_{\text{reference tracks}}}. \tag{2.1}$$

For the *cluster efficiency*, which can be determined for each sensor of the module individually, a reference track is matched to a cluster of DUT hits on each sensor if

$$|x_{\text{cluster}}, x_{\text{track}}| \leqslant 200\ \mu\text{m} \tag{2.2}$$

is fulfilled, where x_{cluster} and x_{track} denote the cluster and track position. The stub efficiency is determined by combining the hits of both sensor layers applying two cuts for the track matching

2023 JINST 18 C01005

$$\text{seed layer: } |x_{\text{stub}}, x_{\text{track}}| \leqslant 200\ \mu\text{m} \tag{2.3}$$

$$\text{correlation layer: } |x_{\text{stub + stub bend}}, x_{\text{track}}| \leqslant 200\ \mu\text{m}. \tag{2.4}$$

The probability to detect one noise hit per triggered readout and channel is given by the *noise occupancy*, which is measured for different thresholds in absence of external signals.

3 Results

All measurements shown in this section have been performed at a sensor bias voltage of 600 V, which is the anticipated nominal operation voltage of the sensors for the Outer Tracker. The threshold applied to the CBC chips reading out the sensor signals is given in ADC units called V_{CTH} and is translated to an equivalent electron charge using a conversion factor of $1V_{\text{CTH}} = 156\ \text{e}^-$.

3.1 Threshold scan and instrip efficiency

The cluster efficiency and noise occupancy measured with different modules in dependence of the threshold is shown in the left plot of figure 3. Prior to irradiation, the efficiency forms a plateau well above 99.5% for thresholds up to 10 ke$^-$. In contrast, the efficiency of the irradiated sensors decrease significantly with increasing threshold. Furthermore, a general difference in the global cluster efficiency of the irradiated sensors can be observed. Higher fluence results in an overall lower efficiency. At the maximum tested fluence, efficiencies above 99.5% can only be reached for thresholds below 4.7 ke$^-$.

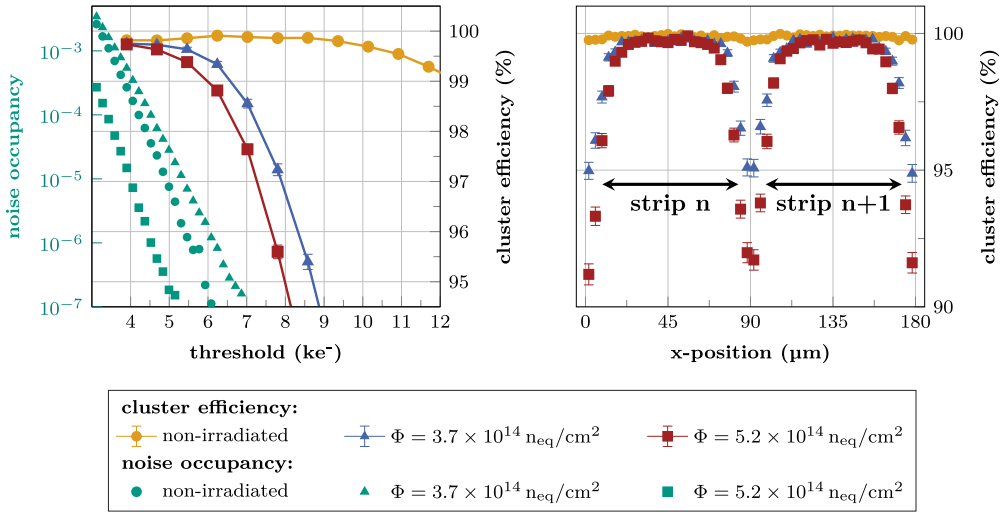

Figure 3. Left: noise occupancy (left *y*-axis) and cluster efficiency (right *y*-axis) of differently irradiated sensors measured in dependence of the threshold. Right: position dependent cluster efficiency of two neighboring strips measured at 7 ke$^-$ threshold. The measurements shown in both plots have been performed at a sensor bias voltage of 600 V.

2023 JINST 18 C01005

For optimal module operation, the noise occupancy should be several orders of magnitudes smaller than the channel occupancy, which is expected to be about 1% during the HL-LHC phase [9]. Taking 1×10^{-4} as a baseline for the upper noise occupancy limit, the threshold that has to be applied for the non-irradiated and medium irradiated sensor is in the order of 4 ke$^-$ to 4.5 ke$^-$. These threshold values are close to the thresholds where the cluster efficiency of the irradiated sensors begins to decrease. Thus, reducing the noise occupancy would increase the safety margin for efficient hit detection. High noise levels, especially for the module bottom sensor, is a known problem of the latest 2S prototype modules and is not related to the irradiation. This can be seen by the fact that the noise occupancy of the sensor with the highest fluence, the top sensor of the irradiated module, is lower compared to the noise occupancy of the sensor with the lower fluence, the bottom sensor. Additionally, the noise is temperature dependent and therefore, the noise occupancy of the highly irradiated sensor is even lower than the noise occupancy measured with the top sensor of the non-irradiated module as the irradiated module has been operated at about −20 °C. The Outer Tracker collaboration is intensively working on mitigating the noise. Significant progress has been achieved.

Inefficient sensor regions between the strips can be identified by superimposing all illuminated strips within one plot resulting in increased statistics. Efficiency projections along two neighboring strips for the differently irradiated sensors measured at a threshold of 7 ke$^-$ are depicted on the right side of figure 3. Prior to irradiation, no inefficient areas are observed. Reduced efficiencies after irradiation mainly originate from the interstrip region, where two aspects have to be taken into account. Firstly, the overall readout signal is reduced due to temporary charge trapping caused by defects in the silicon lattice introduced by irradiation, and secondly, the generated charge at the interstrip region is shared between two neighboring strips. The combination of both effects results in a significantly decreased efficiency at the interstrip region after irradiation for perpendicular tracks.

3.2 Module performance at inclined particle incidence

The functionality of the stub logic, explained in section 1, can be validated by rotating the module with respect to the beam, emulating particles with varying transverse momenta that are differently bent by the magnetic field. Figure 4 shows the resulting stub efficiency curves measured with the non-irradiated and irradiated module. At small rotation angles the displacement of the particle hit position in the correlation layer with respect to the seed signal is small and, thus, within the correlation window. The resulting stub efficiency plateaus show efficiency values above 99% for both modules. By further increasing the module rotation angle, the relative hit displacement between the sensor layers becomes larger, and the correlation condition defined by the correlation window is no longer fulfilled. Hence, the stub efficiency sharply drops to 0%. To directly compare the individual stub efficiency turn-on curves the inflection point is used, which is extracted by fitting a sigmoid function to the measurement data. Systematic uncertainties mainly originate from the limited precision of the rotation stage, which is about ±0.05°. Another factor that has to be taken into account is the relative sensor displacement within each module. Alignment precision measurements during the module assembly procedure show that the displacement is smaller than 4 μm, corresponding to an additional inflection angle uncertainty of 0.15°.

2023 JINST 18 C01005

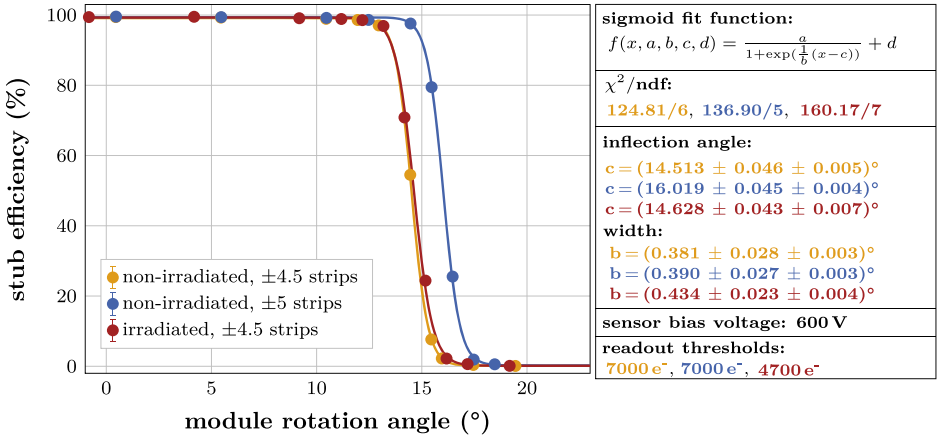

Figure 4. Stub efficiency measured with different modules at varying rotation angles together with the corresponding data fit. Larger correlation windows shift the falling efficiency edge towards higher angles, following the geometrical expectation. The irradiated and non-irradiated module show consistent efficiency turn-on curves for identical window settings.

Different correlation window sizes have been tested with the non-irradiated module. Increasing the window size from ±4.5 strips to ±5 strips shifts the inflection point towards higher angles corresponding to lower p_T. The fit parameter b is a measure of the turn-on widths, which are consistent to each other taking into account the underlying uncertainties. For the non-irradiated module, the sensor spacing at the module middle has been measured to be (1.62 ± 0.02) mm using a high precision microscope. The discrepancy to the intended 1.8 mm sensor spacing originates from the AL-CF bridge prototypes used during module assembly, which were originally designed for different active sensor thicknesses then the ones used for the module. Overall, the extracted inflection angles measured with both window settings are in good agreement with the geometrical expectation based on the measured sensor distance.

Directly comparing the stub identification performance of independently assembled modules measured with the same window settings reveals consistent results considering the given uncertainties. The turn-on curve width measured with the irradiated module appears to be slightly wider compared to the width measured with the non-irradiated module. Based on the data set investigated here, the change in turn on width cannot be unambiguously attributed to irradiation. Small rotations of the two 2S sensors with respect to each other affect the investigated turn-on width as well. However, the impact on the p_T discrimination is negligible and the measurements prove the full functionality of the stub logic.

4 Conclusion

Beam test measurements at DESY with the latest version of 2S module prototypes have been performed by the CMS collaboration. Modules with non-irradiated and irradiated components have been tested to probe the module performance at the beginning and end of the CMS runtime.

2023 JINST 18 C01005

Prior to irradiation and with sensor fluences up to 5.2×10^{14} n_{eq}/cm^2, which is slightly higher than the maximum fluence expected for 2S modules, cluster efficiencies above 99.5% can be reached. The module noise occupancy requires to operate the module close to thresholds where the cluster efficiency of irradiated sensors starts to slightly decrease. Small changes in the module design are required to reduce the noise and to gain longevity, allowing lower readout thresholds for particle detection at maximum cluster efficiency. In the meantime, the source of additional noise has been identified, and a modified service hybrid design is being finalized. Furthermore, the stub logic has been tested by rotating the modules with respect to the beam simulating particle tracks with different transverse momenta. Both modules reach stub efficiencies above 99% for tracks within the correlation window. Different windows sizes were tested, where larger correlation windows result in a shifted efficiency drop towards higher angles, matching the geometrical expectation. Stub efficiency turn on-curves measured with the non-irradiated and irradiated 2S module show consistent shapes for identical correlation window settings.

The measurements presented in this article show that the 2S module design meets the requirements besides the increased noise level, which requires small design optimizations for production readiness.

Acknowledgments

We acknowledge funding by the Federal Ministry of Education and Research of Germany in the framework of the FIS-Projekt Fortführung des CMS-Experiments zum Einsatz am HL-LHC: Verbesserung des äußeren Spurdetektors für das Phase-2-Upgrade des CMS-Experiments'. The measurements leading to these results have been performed at the Test Beam Facility at DESY Hamburg (Germany), a member of the Helmholtz Association (HGF). Furthermore, our gratitude extends to all people from DESY and RWTH Aachen University for their help during the data taking shifts.

References

[1] CMS collaboration, *The CMS experiment at the CERN LHC,* 2008 *JINST* **3** S08004.

[2] D. Contardo et al., *Technical Proposal for the phase-II upgrade of the CMS detector*, Tech. Rep. CMS-TDR-15-02Geneva (2015).

[3] K. Uchida et al., *The CBC3 readout ASIC for CMS 2S-modules*, Tech. Rep. CMS-CR-2018-017 CERN, Geneva (2018).

[4] lpGBT Team, *lpgbt Manual* (2021) https://lpgbt.web.cern.ch/lpgbt/v0/.

[5] L. Olantera et al., *Versatile link+ transceiver production readiness, PoS TWEPP2019 055* (2020).

[6] CERN, *bPOL12V_V6 radiation tolerant 10 W synchronous step-down buck DC/DC converter* (2022).

[7] CERN, *bPOL2V5_V3.3 radiation tolerant synchronous step-down buck DC/DC converter* (2022).

[8] M. Pesaresi and G. Hall, *Simulating the performance of a p_T tracking trigger for CMS,* 2010 *JINST* **5** C08003.

2023 JINST 18 C01005

[9] CMS collaboration, *The phase-2 upgrade of the CMS tracker*, Tech. Rep. CMS-TDR-014CERN, Geneva (2017).

[10] ZAG Zyklotron AG, https://zyklotron-ag.de/.

[11] R. Diener et al., *The DESY II test beam facility, Nucl. Instrum. Meth. A* **922** (2019) 265.

[12] H. Jansen et al., *Performance of the EUDET-type beam telescopes, EPJ Techn. Instrum.* **3** (2016) 7.

[13] Y. Liu et al., *EUDAQ2-A flexible data acquisition software framework for common test beams,* 2019 *JINST* **14** P10033.

[14] T. Bisanz et al., *EUTelescope: a modular reconstruction framework for beam telescope data,* 2020 *JINST* **15** P09020.

[15] C. Kleinwort, *General broken lines as advanced track fitting method, Nucl. Instrum. Meth. A* **673** (2012) 107.

2023 JINST 18 C01005